Symmetry breaking in a localized interacting binary Bose-Einstein condensate in a bichromatic optical lattice

Yongshan Cheng[1,2,*] and S. K. Adhikari[1,†]

[1]*Instituto de Física Teórica, UNESP—Universidade Estadual Paulista, 01.140-070 São Paulo, Brazil*

[2]*Department of Physics, Hubei Normal University, Huangshi 435002, People's Republic of China*

(Received 24 November 2009; published 24 February 2010)

By direct numerical simulation of the time-dependent Gross-Pitaevskii equation using the split-step Fourier spectral method, we study different aspects of the localization of a cigar-shaped *interacting* binary (two-component) Bose-Einstein condensate (BEC) in a one-dimensional bichromatic quasiperiodic optical-lattice potential, as used in a recent experiment on the localization of a BEC [Roati *et al.*, Nature **453**, 895 (2008)]. We consider two types of localized states: (i) when both localized components have a maximum of density at the origin $x = 0$, and (ii) when the first component has a maximum of density and the second a minimum of density at $x = 0$. In the noninteracting case, the density profiles are symmetric around $x = 0$. We numerically study the breakdown of this symmetry due to interspecies and intraspecies interactions acting on the two components. Where possible, we have compared the numerical results with a time-dependent variational analysis. We also demonstrate the stability of the localized symmetry-broken BEC states under small perturbation.

DOI: 10.1103/PhysRevA.81.023620 PACS number(s): 03.75.Nt, 03.75.Lm, 64.60.Cn, 67.85.Hj

I. INTRODUCTION

After the prediction of the localization of the electronic wave function in a disordered potential by Anderson 50 years ago [1], there have been many studies on different aspects of localization of different types of waves, e.g., electron, sound, and electromagnetic waves [2–4], and quantum-matter waves in the form of a Bose-Einstein condensate (BEC) [5–8]. In the case of a quantum-matter wave, a disordered speckle potential [5] and a quasiperiodic bichromatic optical lattice (OL) potential [6] have been employed for the localization of a noninteracting cigar-shaped BEC. The quasiperiodic bichromatic OL potential was formed by the superposition of two standing-wave polarized laser beams with incommensurate wavelengths. Each standing-wave polarized laser beam leads to a periodic OL potential. The noninteracting BEC of ^{39}K atoms was created [6] by tuning the interatomic scattering length to zero near a Feshbach resonance [9].

The localization of a cigar-shaped BEC in a one-dimensional (1D) bichromatic OL potential and related topics have been the subject matter of several theoretical [10–19] and experimental [5–8] studies. (Localized BEC states in the form of a gap soliton in a mono-chromatic OL potential have also been observed [20] and studied [21]. However, there are fundamental differences between the two types of localized states. The Anderson localized states in a bichromatic OL potential appear predominantly in the linear Schrödinger equation and are destroyed above a small critical repulsive nonlinearity, whereas the gap solitons appear only in the presence of a repulsive nonlinearity. The linear system does not support a localized gap soliton. The gap solitons appear in the band gap of the spectrum of the periodic OL potential. On the other hand, the potential supporting the Anderson states must be aperiodic in nature.) After the pioneering experiments [5,6] on the localization of a 1D cigar-shaped noninteracting BEC, a natural extension of this phenomenon would be to investigate localization in a weakly interacting binary (two-component) BEC mixture.

In this paper, with intensive numerical simulations of the Gross-Pitaevskii (GP) equation, we study different aspects of localization of a cigar-shaped binary BEC in a 1D bichromatic quasiperiodic OL potential—similar to the one used in the experiment of Roati *et al.* [6]. Although most of the studies of Anderson localization were confined to noninteracting systems, in the present study on the localization of a two-component BEC we shall mostly consider a weakly interacting system under the action of both interspecies and intraspecies interactions. If the potential $V(x)$ is symmetric around origin at $x = 0$, e.g., $V(x) = V(-x)$, for the noninteracting system, the density profiles are symmetric around $x = 0$: $|u(x)|^2 = |u(-x)|^2$, where $u(x)$ is the wave function of the matter wave. But for the interacting system with inter- and intraspecies interaction, this symmetry can be broken and different types of symmetry-broken states emerge, and we shall be specially interested in the study of the formation of localized cigar-shaped BEC components with broken symmetry.

The two components of the BEC could be two different hyperfine states of the same atom [22] or two different atoms [23], and the two confining bichromatic OL potentials for the two components could be the same or different [6,12,14]. The bichromatic OL potential could be taken as the linear combination of two sine terms, both with a minimum at the origin ($x = 0$), when the confined BEC components will have a maximum at the origin. The bichromatic OL potential could also be taken as the linear combination of two cosine terms with a maximum at the origin, while the confined BEC components will have a minimum at the origin. We shall consider two distinct situations of localized binary BEC: (i) two components under the action of the identical sine bichromatic OL potential while both densities have maxima at $x = 0$, and (ii) component 1 under the action of the sine bichromatic OL potential with a maximum of density at $x = 0$ and component 2 under the action of the cosine bichromatic OL potential with a minimum of density at $x = 0$.

*yong_shan@163.com

†adhikari@ift.unesp.br; URL: www.ift.unesp.br/users/adhikari

In case (i), with weak interspecies and intraspecies repulsions, the localized BEC components are overlapping with a maximum at $x = 0$. But under the action of a interspecies repulsion above a critical value, the two repealing BEC components separate and move to opposite sides of $x = 0$, thus breaking the symmetry around $x = 0$. It is this separation or splitting of the BEC components which we study. (Similar separation of gap solitons [21] in a binary BEC mixture confined by a monochromatic lattice has been studied [24,25].)

In case (ii), a different type of symmetry breaking emerges. In this case, with weak intraspecies and interspecies repulsion or attraction, the localized BEC components have densities symmetric around $x = 0$. But under the action of an interspecies attraction above a critical value, the two attracting BEC components try to stick together as a pair of bright solitons [26], and the minimum-energy stable configuration is the one where both components move predominantly to the same side of $x = 0$, thus breaking the symmetry around $x = 0$. We study this symmetry breaking in detail.

In our study we use the direct numerical simulation of the underlying GP equation using the split-step Fourier spectral method. We also use a time-dependent variational analysis for an analytical understanding of the numerical results in case (i) when both components have a maximum at $x = 0$ with densities having quasi-Gaussian shapes. In this case, certain aspects of the splitting of the two components are also predicted correctly from the variational analysis.

There have already been a number of theoretical and experimental studies on Anderson localization in different problems. The effect of a repulsive nonlinearity on localization of light waves in photonic crystals was studied experimentally [27]. There have also been studies of a weak repulsion on localization [12,14,17,28]. Damski *et al.* and Schulte *et al.* considered Anderson localization in a disordered OL potential [11], whereas Sanchez-Palencia *et al.* and Clément *et al.* considered Anderson localization in a random potential [10]. There have been studies of Anderson localization with other types of disorder [29]. Anderson localization in BEC under the action of a disordered potential in two and three dimensions has also been investigated [30].

In Sec. II, we present a brief account of (i) the two-component 1D GP equation, (ii) the bichromatic OL potentials used in our study, and (iii) a time-dependent variational analysis of the GP equation under appropriate conditions. In Sec. III, we present our numerical studies on localization using the split-step Fourier spectral method. The density profile of the quasi-Gaussian localized states are in agreement with the variational results. The density of the localized states are symmetric around the origin at $x = 0$ in the absence of interspecies interaction. We study the symmetry breaking under the action of an interspecies interaction. Certain aspects of symmetry breaking can be explained with the variational analysis. We also demonstrate the dynamical stability of the two-component localized states. In Sec. IV, we present a brief discussion and concluding remarks.

II. ANALYTICAL CONSIDERATION OF LOCALIZATION

We consider a two-component cigar-shaped BEC under tight transverse harmonic confinement with the bichromatic OL potential acting along the axial x direction. Then it is appropriate to consider a 1D reduction [31] of the 3D GP equation by freezing the transverse dynamics to the respective ground state and integrating over the transverse variables. Such a binary BEC is described by the following coupled 1D BEC equations [24,31]:

$$i\frac{\partial u_1}{\partial t} = -\frac{1}{2}\frac{\partial^2 u_1}{\partial x^2} + g_1|u_1|^2 + g_{12}|u_2|^2 u_1 + V_1(x)u_1, \quad (1)$$

$$i\frac{\partial u_2}{\partial t} = -\frac{1}{2}\frac{\partial^2 u_2}{\partial x^2} + g_2|u_2|^2 + g_{12}|u_1|^2 u_2 + V_2(x)u_2, \quad (2)$$

with normalization $\int_{-\infty}^{\infty}|u_j|^2 dx = 1$, of the localized wave function u_j of the two components $j = 1, 2$. Because the localization of the BEC in the bichromatic lattice is most prominent for the linear problem, we shall be interested in only small nonlinearities g_1, g_2 and g_{12}. To make the parameters of the model tractable, we take the number of atoms N_j and the mass m_j of the two components to be equal: $N_1 = N_2 = N$ and $m_1 = m_2 = m$. This simplification will have no effect on the general conclusion of this study. The intraspecies nonlinearities are given by [31] $g_j = 2a_j N/a_\perp$, $a_\perp \equiv \sqrt{\hbar/(m\omega)}$, and $\omega \equiv \sqrt{\omega_y\omega_z}$, where ω_y and ω_z are the transverse trap frequencies in the y and z directions, respectively, and a_j is the intraspecies atomic scattering length. The interspecies nonlinearity is given by [31] $g_{12} = 2Na_{12}/a_\perp$, where a_{12} is the interspecies scattering length. In Eqs. (1) and (2), $V_j(x)$ are the bichromatic OL traps of the two components $j = 1, 2$. Here we are using harmonic oscillator units: length is expressed in units of transverse oscillator length $a_\perp$ and time in units of angular frequency $(\omega)^{-1}$.

In the first part of our study, we shall take the two bichromatic OL potentials to be identical, that is, $V_1(x) = V_2(x) = V(x)$, and having the following sine form as in the experiment [6]:

$$V(x) = \sum_{l=1}^{2} A_l \sin^2(k_l x), \quad (3)$$

with $A_l = 2\pi^2 s_l/\lambda_l^2$, where λ_l are the wavelengths of the laser forming the OL potentials, s_l are their intensities, and $k_l = 2\pi/\lambda_l$ the corresponding wave number.

In the second part of our study, we shall take $V_1(x)$ to be given by Eq. (3), whereas in $V_2(x)$ the sine term is replaced by a cosine term:

$$V_2(x) = \sum_{l=1}^{2} A_l \cos^2(k_l x). \quad (4)$$

Potentials (3) and (4) are quite similar. However, potential (4) generates a different type of localized state compared to potential (3). Potential (3) has a local minimum at the center $x = 0$; consequently, stable stationary solutions with this potential have a maximum at $x = 0$. However, potential (4) has a local maximum at $x = 0$ corresponding to a minimum of the stationary solution at the center.

With a single periodic potential of the form $\sin^2(2\pi x/\lambda)$ or $\cos^2(2\pi x/\lambda)$ with $s_2 = 0$, the linear Schrödinger equation permits only delocalized states in the form of Bloch waves.

Localization is possible in the linear Schrödinger equation due to the "disorder" introduced through a second component in Eq. (3) or (4). The primary lattice is usually strong enough and is used as the main periodic potential fixing the Bloch band structure of the single-particle states without disorder. The secondary lattice is weaker ($s_2 \ll s_1$) and introduces a "deterministic" disorder. Following the experiment of Roati *et al.* [6], the transverse harmonic-oscillator length is of the order of a few microns, so the wavelengths of the OL in dimensionless units become approximately $10^0 \sim 10^1$.

Usually, the stationary BEC localized states formed with bichromatic lattices occupy many sites of the quasiperiodic OL potential, and their shape is modulated by the short-wavelength potential [32]. For certain values of the parameters, potential (3) leads to bound states confined practically to the central site of the quasiperiodic OL potential. When this happens, a variational approximation with Gaussian ansatz leads to a reasonable prediction for the bound state. To apply the variational approach with potential (3) effective on both components, we adopt the Gaussian function below as the variational ansatz [33]:

$$u_j(x,t) = \frac{1}{\pi^{1/4}}\sqrt{\frac{\mathcal{N}_j}{w_j}}\exp\left[-(x-x_{0j})^2/\left(2w_j^2\right)\right] \times \exp[i\{C_j(x-x_{0j})+\phi_j\}], \tag{5}$$

where w_j are the widths of component j of localized BEC centered at x_{0j}, ϕ_j is the corresponding phase, C_j is the linear phase coefficient, and $\mathcal{N}_j$ is the normalization of component j. We shall consider the solution where the widths are comparable to the OL wavelength. Generally, the variational approach is valid when the OL is only smooth and slowly varying on the localized states scale [32]. We shall obtain useful relations among the variational parameters of the localized BEC states. This will allow us to get a better physical understanding of the localized states.

The GP equations (1) and (2) can be derived from the Lagrangian

$$L(t) = \int_{-\infty}^{\infty}\left\{\sum_{j=1}^{2}\left(\frac{i}{2}[u_j^*\dot{u}_j - u_j\dot{u}_j^*] - \frac{1}{2}[|u_j'|^2 + g_j|u_j|^4] - V(x)|u_j|^2\right) - g_{12}|u_1|^2|u_2|^2\right\}dx, \tag{6}$$

where the overhead dot denotes time derivative, the star denotes complex conjugation, and the prime denotes space derivative. Using ansatz (5) in Eq. (6), we get

$$L(t) = \sum_{j=1}^{2}\mathcal{N}_j\left[(C_j\dot{x}_{0j} - \dot{\phi}_j) - \frac{1}{2}\left(\frac{1}{2w_j^2} + C_j^2\right) - \frac{g_j\mathcal{N}_j}{2\sqrt{2\pi}w_j} + \sum_{l=1}^{2}L_{lj}\right] + L_{12}, \tag{7}$$

$$L_{12} \equiv -\int_{-\infty}^{\infty} g_{12}|u_1|^2|u_2|^2\,dx = -\frac{g_{12}\mathcal{N}_1\mathcal{N}_2}{\sqrt{\pi\left(w_1^2+w_2^2\right)}}\exp\left(-\frac{\rho^2}{w_1^2+w_2^2}\right), \tag{8}$$

$$L_{lj} \equiv \frac{A_l}{2}\left[\cos(2k_lx_{0j})\exp\left(-k_l^2w_j^2\right) - 1\right], \tag{9}$$

where $\rho = x_{02} - x_{01}$, and the variational parameters are the norm $\mathcal{N}_j$, width w_j, position x_{0j}, and phase parameters C_j and ϕ_j. We use the Euler-Lagrange equation

$$\frac{\partial L}{\partial\sigma} - \frac{d}{dt}\frac{\partial L}{\partial\dot{\sigma}} = 0, \tag{10}$$

where σ is the variational parameter. The first variational equation using $\sigma = \phi_j$ yields $\mathcal{N}_j =$ constant. Without losing generality, we shall take this constant to be unity and use it in the subsequent equations. Taking $\sigma = x_{0j}, C_j, w_j$, and $\mathcal{N}_j$, respectively, we obtain the following equations

$$\dot{C}_j = \frac{\partial}{\partial x_{0j}}\left(\sum_{l=1}^{2}L_{lj} + L_{12}\right), \tag{11}$$

$$\dot{x}_{0j} = C_j, \tag{12}$$

$$\frac{1}{w_j} + \frac{g_j}{\sqrt{2\pi}} + \frac{2g_{12}w_j^3}{\sqrt{\pi}\left(w_1^2+w_2^2\right)^{3/2}}\left(1 - \frac{2\rho^2}{w_1^2+w_2^2}\right)\exp\left(-\frac{\rho^2}{w_1^2+w_2^2}\right) - \sum_{l=1}^{2}2A_lw_j^3k_l^2\cos(2k_lx_{0j}) \times \exp\left(-k_l^2w_j^2\right) = 0, \tag{13}$$

$$\dot{\phi}_j = \frac{C_j^2}{2} - \frac{1}{4w_j^2} - \frac{g_j}{w_j\sqrt{2\pi}} + \left.\frac{\partial L_{12}}{\partial\mathcal{N}_j}\right|_{\mathcal{N}_j=1} + \sum_{l=1}^{2}L_{lj}. \tag{14}$$

The set of equations (11)–(14) shows that the phase ϕ_j has no effect on the location x_{0j}, width w_j, and the coefficient C_j of solitons, whereas it is determined by the variational equation (14). Hence we shall neglect Eq. (14) in the following and consider only Eqs. (11)–(13). (However, we could not set phase $\phi_j = 0$ in the beginning, as the Euler-Lagrange equation for ϕ_j leads to the important result of norm conservation.) Equation (13) determines the width w_j in terms of nonlinearities g_j, g_{12} and the parameters of the bichromatic OL potential. The density distribution is quasi-Gaussian only for small values of x_{0j}, and we shall be limited to this constraint (small $|x_{0j}|$) while considering the variational approach. In the symmetric case, while $g_1 = g_2$, the widths of the two localized states are equal. However, when $g_1 \neq g_2$, the widths of the two localized states are not equal, and one has two asymmetric localized states. When $x_{01} = x_{02} = 0$, the widths of the two stationary BEC localized states are determined by

$$\frac{1}{w_j} + \frac{g_j}{\sqrt{2\pi}} + \frac{2g_{12}w_j^3}{\sqrt{\pi}\left(w_1^2+w_2^2\right)^{3/2}} - \sum_{l=1}^{2}2A_lw_j^3k_l^2\exp\left(-k_l^2w_j^2\right) = 0. \tag{15}$$

Now we obtain, following Ref. [34], the equation of motion describing the center of the two BEC localized states as if they were a particle in an effective potential. Thus, we can determine the motion of equivalent particles using the classical mechanics analogy. Inserting Eqs. (8), (9), and (11) into Eq. (12), we obtain the following equation for dynamics:

$$\frac{d^2x_{0j}}{dt^2} = -\frac{\partial V_{\mathrm{eff}\,j}}{\partial x_{0j}}\,, \tag{16}$$

$$V_{\mathrm{eff}\,j} = \frac{g_{12}}{\sqrt{\pi\left(w_1^2+w_2^2\right)}}\exp\left(-\frac{\rho^2}{w_1^2+w_2^2}\right) - \sum_{l=1}^{2}\frac{A_l}{2}\left[\cos(2k_l x_{0j})\exp\left(-k_l^2 w_j^2\right)-1\right], \tag{17}$$

where the anharmonic effective potentials $V_{\mathrm{eff}\,j}$ are the dynamic potentials for the movement of the center of the localized BECs and depend on characteristics of the two BEC localized states (e.g., width w_j and position x_{0j}) and potential parameters (e.g., k_l and A_l). The effective potentials have two parts. The first term on the right of Eq. (17) is induced by the mutual interaction of the two BEC localized states. When the coupling constant $g_{12} > 0$, it is positive and contributes to a repulsive potential barrier for BEC localized states. The second term in Eq. (17) arises from the bichromatic OL potential and contributes to an attractive potential well, if $|x_{0j}|$ is small enough. The combination of the two terms may lead to local minima or local maxima at the origin $x_{0j} = 0$ in the effective potential $V_{\mathrm{eff}\,j}$.

When the two BEC localized states are symmetrical ($g_1 = g_2$), they will feel the same effective potential. In that case, we should have $w_1 = w_2 = w$ and $x_{01} = -x_{02} = x_0$. The effective potential V_{eff} is plotted in Fig. 1(a) vs x_0 in the symmetric case $g_1 = g_2 = 0$ for different interspecies interaction: $g_{12} = 0.5$, 1, and 3. Equation (13) is first solved to find w as a function of x_0. This result is then substituted in Eq. (17) to find $V_{\mathrm{eff}}(x_0)$ as plotted in Fig. 1(a). From Fig. 1(a), we find that if g_{12} is smaller, the effective potential possesses a local minimum at $x_0 = 0$. In this case, if we start with two BEC localized states at $x = 0$ for small g_{12}, they will be in stable equilibrium and unsplit. The effective potential becomes weaker, with the local minimum at $x_0 = 0$ less pronounced as g_{12} increases. If g_{12} is large enough [e.g., $g_{12} = 3$ in Fig. 1(a)], a local maximum appears in the effective potential at $x_0 = 0$; and the peak value at maximum increases as g_{12} increases. In this case, two overlapping (unsplit) initial localized BEC states at the maximum at $x = 0$ will be in a metastable configuration. When they are slightly perturbed, for example, by slightly moving the BEC center(s) from $x = 0$, they will move, respectively, toward the minima of the effective potential next to the maximum and split into two nonoverlapping BECs localized at the two local minima of the effective potential on both sides of $x_0 = 0$, as we shall see in Sec. III A.

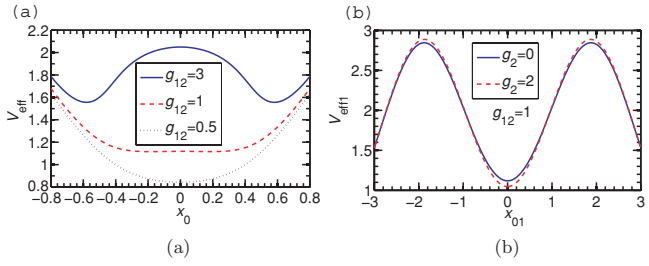

FIG. 1. (Color online) (a) The effective potential $V_{\mathrm{eff}}(x_0)$ vs the position of the localized state $x_0 \equiv x_{01} = -x_{02}$ in the symmetric case $g_1 = g_2 = 0$ for $g_{12} = 0.5$, 1, and 3 as obtained from Eq. (17). The respective widths are calculated from Eq. (13). (b) The effective potential felt by the first component $V_{\mathrm{eff1}}(x_{01})$ vs its position x_{01} as obtained from Eq. (17). The widths of the two states are calculated from Eq. (15). In both (a) and (b), the potential parameters are $\lambda_1 = 8$, $\lambda_2 = 0.862\lambda_1$, $s_1 = 8$, and $s_2 = 2.4$.

When the two BEC localized states are asymmetrical ($g_1 \neq g_2$), they will feel different effective potentials. It is difficult to calculate these effective potentials exactly. But we can calculate the effective potential(s) (17) under simplifying assumptions. The widths w_1 and w_2 are assumed to be independent of positions x_{01} and x_{02} and were calculated using Eq. (15) and substituted into Eq. (17). The function $V_{\mathrm{eff1}}(x_{01})$ so obtained is plotted in Fig. 1(b) vs x_{01}, for $g_1 = 0$, $g_{12} = 1$, and $g_2 = 0$ and 2. The effective potential acting on component 1 is stronger as g_2 is increased from 0 to 2. This will lead to a reduction of the width of the corresponding localized state as g_2 is increased from 0 to 2, as we shall see in Sec. III A.

III. NUMERICAL RESULTS

We perform the numerical simulation employing the real-time split-step Fourier spectral method with space step 0.04, time step 0.001. (We also checked the results using the real-time Crank-Nicolson discretization routine, the FORTRAN programs which are given in Ref. [35].) Because of the oscillating nature of the potential, great care was needed to obtain a precise localized state. The accuracy of the numerical simulation was tested by varying the space and time steps as well as the total number of space steps. The initial input pulse is a Gaussian wave packet, $u_j(x, t = 0) = \pi^{-1/4}\exp(-x^2/2)$ with a parabolic trap $V'(x) = x^2/2$. Let $g_1 = g_2 = g_{12} = 0$, and the coupled Eqs. (1) and (2) become the linear Schrödinger equation. To start the numerical simulation, the parabolic trap is slowly turned off and the bichromatic OL is slowly turned on; the increment in the coefficient s_i in each time step is 0.00005. Successively, we add gradually the nonlinear coefficient g_2 and the coupling constant g_{12} slowly. The increment of g_2 and g_{12} is 0.00001 in each time step. Thereby the stationary localized states are obtained.

To perform a systematic numerical study of localization, we take $s_1 = 8$, $s_2 = 2.4$, $\lambda_1 = 8$, and $\lambda_2 = 0.862\lambda_1$, maintaining the ratio $\lambda_2/\lambda_1 = 0.862$ similar to the value employed in the experiment [6]. The values of s_1 and s_2 are also in the range employed in the experiment. With this set of parameters and for weak interspecies and intraspecies interactions, the localized BEC state could be mostly confined in the single cell of the bichromatic OL potential. All results reported here are obtained with these potential parameters, except for those in Figs. 3(e) and 3(f), where we study the effect of the change of potential parameters. We consider a transverse harmonic oscillator length $a_\perp \approx 1$ μm, so that the wave lengths of the

OL potential are approximately 800 and 689 nm. We shall take $g_1 = 0$ throughout the present investigation.

A. Localized states with potential (3) on both components

We start the numerical analysis with a consideration of the widths of the two components of the localized BECs with potential (3) acting on both components. In this case, both components could have a maximum at the center $x = 0$ with localized states of quasi-Gaussian forms, and when this happens the system can be described well by the variational approximation. Assuming a Gaussian distribution for the localized BEC, the numerical width is calculated via

$$w_j^2 = 2\int_{-\infty}^{\infty} |u_j|^2 x^2\, dx. \tag{18}$$

The numerical and variational results for the widths w_j vs g_2 for $g_{12} = 1$ are plotted in Fig. 2(a). The same for $g_2 = 0.5$ vs g_{12} are plotted in Fig. 2(b). In these plots, there is reasonable agreement between the numerical and variational results for the width, and the width usually increases with the increase of nonlinearities g_2 and g_{12} except in the case of w_1 in Fig. 2(a). The general increase of width with the increase of nonlinearity (increase of repulsion) is expected; however, the decrease of w_1 with g_2 in Fig. 2(a) requires special attention. This phenomenon will be clear if we consider the effective potential of component 1 as illustrated in Fig. 1(b) when g_2 is changed from 0 to 2. We find that the effective potential becomes slightly stronger as g_2 increases corresponding to a reduction of width w_1 in Fig. 2(a) with the increase of g_2.

Next we consider typical numerical profiles of the densities of the localized BEC states $|u_j|^2$ and compare them with variational results for small values of g_{12} when the centers of both components are at the origin: $x_{01} = x_{02} = 0$. In Figs. 3(a) and 3(b), we present the results for $g_1 = g_2 = 0$ and $g_{12} = 0$ and 1, respectively, while the two density profiles $|u_1|^2$ and $|u_2|^2$ are equal. Next we consider results for the asymmetric case while $g_1 \neq g_2$ while the two densities are different. In Figs. 3(c) and 3(d), we present the results for $g_1 = 0$, $g_2 = 1$, and $g_{12} = 2$ and for $g_1 = 0$, $g_2 = 2$, and $g_{12} = 1$, respectively. In both cases, the component 1 is more strongly localized in space with a smaller width. Next we consider the effect of a variation of the wavelengths λ_1 and λ_2 on the densities. In Fig. 3(e) we plot the densities for $\lambda_1 = 10$ and $\lambda_2 = 0.862\lambda_1$, and in Fig. 3(f) we plot the densities for $\lambda_1 = 5$ and $\lambda_2 = 0.862\lambda_1$; in both cases, we take $g_1 = 0$, $g_2 = g_{12} = 1$, $s_1 = 8$, and $s_2 = 2.4$. In Fig. 3(e), with the increase of λ_l, the central OL site has a larger spatial extension; consequently, the densities have a smaller value at the maxima at the origin corresponding to a larger width. In Fig. 3(f), with the decrease of λ_l, the central OL site has a smaller spatial extension; consequently, the densities have a larger value at the maxima at the origin corresponding to a smaller width.

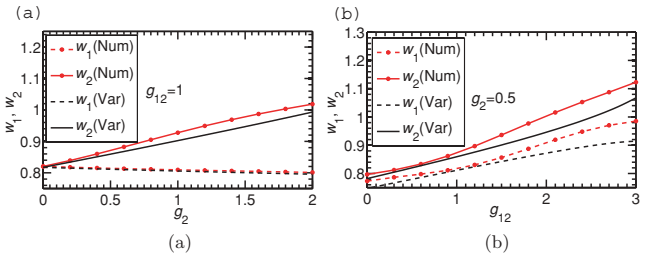

FIG. 2. (Color online) The numerical and variational widths w_1 and w_2 of the two stationary BEC localized states vs (a) g_2 for $g_{12} = 1$ and $g_1 = 0$ and (b) g_{12} for $g_2 = 0.5$ and $g_1 = 0$. The potential (3) acts on the two components where the parameters are $\lambda_1 = 8$, $\lambda_2 = 0.862\lambda_1$, $s_1 = 8$, and $s_2 = 2.4$.

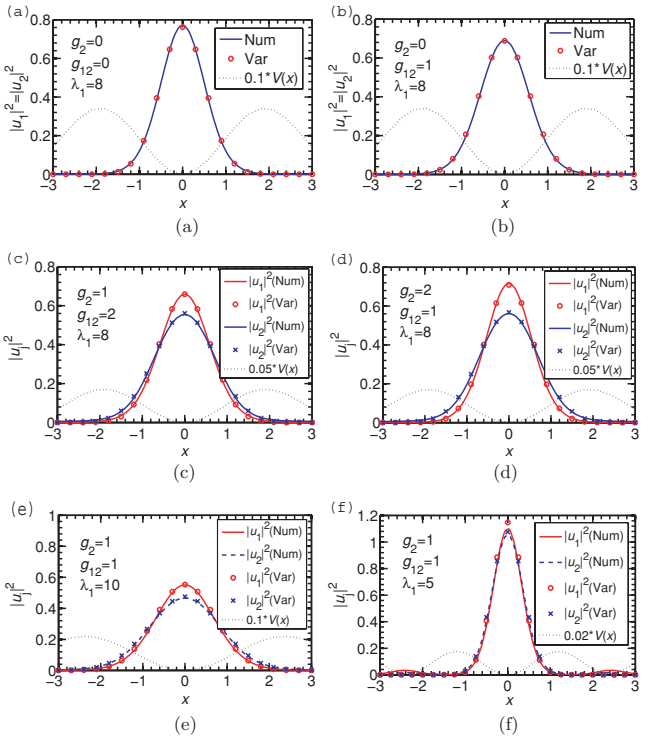

FIG. 3. (Color online) The densities $|u_1(x)|^2$ and $|u_2(x)|^2$ of the two localized BEC states vs x for (a) $g_1 = g_2 = g_{12} = 0$; (b) $g_1 = g_2 = 0$ and $g_{12} = 1$; (c) $g_1 = 0$, $g_2 = 1$, and $g_{12} = 2$; (d) $g_1 = 0$, $g_2 = 2$, and $g_{12} = 1$. In (a)–(d), potential (3) acts on the two components with parameters $\lambda_1 = 8$, $\lambda_2 = 0.862\lambda_1$, $s_1 = 8$, and $s_2 = 2.4$. The last two plots are for $g_1 = 0$ and $g_2 = g_{12} = 1$ with potential parameters (e) $\lambda_1 = 10$, $\lambda_2 = 0.862\lambda_1$, $s_1 = 8$, and $s_2 = 2.4$, and (f) $\lambda_1 = 5$, $\lambda_2 = 0.862\lambda_1$, $s_1 = 8$, and $s_2 = 2.4$. In each case, the profile of the bichromatic OL potential is also shown.

The plots in Figs. 3(a)–3(e) indicate that the numerical results for densities are in perfect agreement with the variational results. They also indicate the good accuracy of the numerical routine. In these cases, the density has a quasi-Gaussian profile used in the variational analysis. In Fig. 3(f), the numerical densities have secondary maxima on both sides of the central peak, the profile deviates from the Gaussian, and there is only fair agreement with the variational results in this case.

So far we presented results in the asymmetric case for small values of g_{12} where the two localized states are overlapping (unsplit) and centered at $x = 0$. As g_{12} increases, it is clear from Fig. 1(a) that the effective potentials experienced by the components develop a maximum at the origin. Hence the position $x = 0$ ceases to be one of stable equilibrium for the components. Consequently, the two localized BECs move on

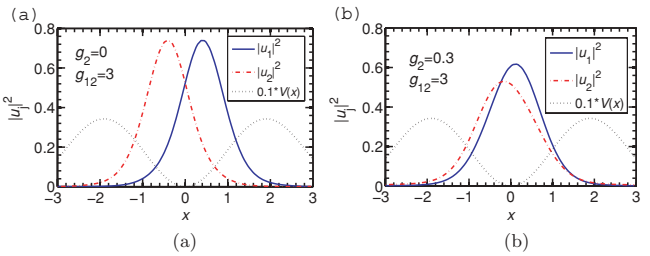

FIG. 4. (Color online) The same as in Fig. 3, but for (a) $g_1 = g_2 = 0$ and $g_{12} = 3$, and (b) $g_1 = 0$, $g_2 = 0.3$, and $g_{12} = 3$. The parameters of the potential are $\lambda_1 = 8$, $\lambda_2 = 0.862\lambda_1$, $s_1 = 8$, and $s_2 = 2.4$.

opposite sides of the point $x = 0$ to attain split (separated) configurations of stable equilibrium. We illustrate this in the symmetric case in Fig. 4(a) for $g_1 = g_2 = 0$ and $g_{12} = 3$, where we plot the densities of the two split components. The two densities continue to be symmetric: $|u_1(x)|^2 = |u_2(-x)|^2$ with centers at $|x_{01}| = |x_{02}| = 0.45$. From Fig. 1(a), we find that the minima of the effective potential for the same set of parameters as in Fig. 4(a) are at $|x_{01}| = |x_{02}| = 0.58$, indicating the centers of the split solitons to be at ± 0.58. The variational analysis is valid for small splitting, and considering that the value ± 0.58 indicating splitting is not too small compared to the extension of the localized states, the agreement between the numerical displacement 0.45 of the localized state and its variational estimate of 0.58 should be considered satisfactory. In Fig. 4(b), we present an example of the localized asymmetric split states for $g_1 = 0$, $g_2 = 0.3$, and $g_{12} = 3$, where the two states have different (asymmetric) densities.

As the split and the unsplit configurations of the localized states are of interest, it is appropriate to represent the split and unsplit configurations in a g_2 vs g_{12} phase diagram for $g_1 = 0$. This is illustrated in Fig. 5. (A similar split-unsplit phase diagram has also been studied in the context of symbiotic gap solitons [24].) For small g_{12}, as expected, the localized states are in an overlapping (unsplit) configuration. The split configuration is achieved when g_{12} is larger than a critical value indicating a minimum of interspecies repulsion needed to move the localized states from $x = 0$. Splitting is favored when the interspecies interaction is strongly repulsive with a large positive value of g_{12} and when the intraspecies interaction

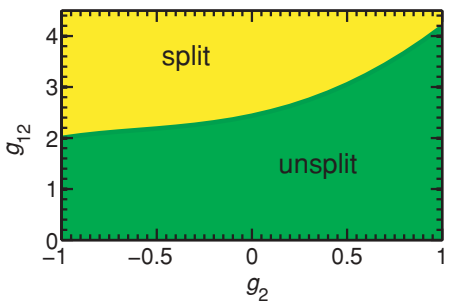

FIG. 5. (Color online) The phase diagram of g_{12} vs g_2 for $g_1 = 0$ showing the split and unsplit configurations of the two localized states while potential (3) is effective on both components. The parameters of the potential are $\lambda_1 = 8$, $\lambda_2 = 0.862\lambda_1$, $s_1 = 8$, and $s_2 = 2.4$.

is attractive corresponding to a negative g_2 as seen in Fig. 5.

B. Localized states with potential (3) on component 1 and potential (4) on component 2

Now we consider the situation when potential (3) acts on component 1 and (4) acts on component 2. In this case, only the first component under the influence of potential (3) could have a maximum at the origin ($x = 0$), and the second component under the influence of potential (4) usually has a minimum at the center; hence the variational approximation is not applicable in this case. (The monochromatic counterpart to this model with the phase-shifted potential (4) was investigated in Ref. [36].) We start our discussion in this case by showing the results of density under different situations. In Fig. 6(a) we plot the densities of the two components for the symmetric noninteracting case for $g_1 = g_2 = g_{12} = 0$. The density $|u_1|^2$ of the first component has a localized Gaussian-type shape centered at $x = 0$. The density of the second component has a two-hump symmetric structure with a minimum at $x = 0$. The symmetry of the densities around $x = 0$ can be broken in the presence of a sufficiently strong interspecies attraction. This is illustrated in Fig. 6(b), where we plot the densities for $g_1 = g_2 = 0$ and $g_{12} = -4$. The center of both densities has moved slightly toward positive x as a sufficiently strong interspecies attraction is introduced via $g_{12} = -4$. In Figs. 6(c) and 6(d), we illustrate the densities in two more cases for $g_1 = 0$, $g_2 = -0.5$, and $g_{12} = -3$, and for $g_1 = 0$, $g_2 = 0.5$, and $g_{12} = -3$, respectively. In Fig. 6(c), the densities are asymmetric; in Fig. 6(d), they are symmetric. This observation is consistent with the general conclusion that symmetry breaking will be favored when the system is attractive. In the case of Fig. 6(c), we have $g_1 = 0$, $g_2 = -0.5$, and $g_{12} = -3$, indicating that both components could be

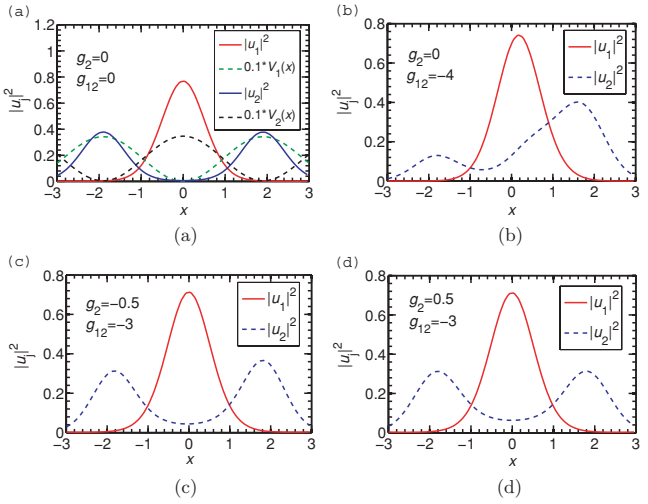

FIG. 6. (Color online) The densities $|u_1(x)|^2$ and $|u_2(x)|^2$ of the two localized BEC states vs x for (a) $g_1 = g_2 = g_{12} = 0$, (b) $g_1 = g_2 = 0$, $g_{12} = -4$, (c) $g_1 = 0$, $g_2 = -0.5$, $g_{12} = -3$, and (d) $g_1 = 0$, $g_2 = 0.5$, $g_{12} = -3$, when potential (3) acts on the first component and potential (4) acts on the second component. The potential parameters are $\lambda_1 = 8$, $\lambda_2 = 0.862\lambda_1$, $s_1 = 8$, and $s_2 = 2.4$.

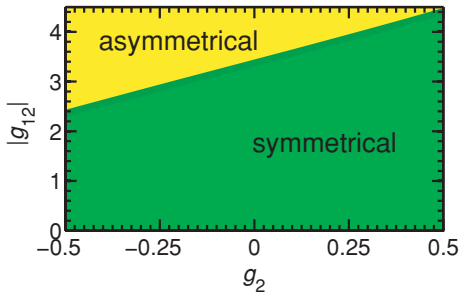

FIG. 7. (Color online) The phase diagram of $|g_{12}|$ vs g_2 for $g_1 = 0$ showing the symmetric and asymmetric configurations of the two localized BEC states. The potential (3) is effective on the first component, and potential (4) on the second component with the same parameters as in Fig. 5.

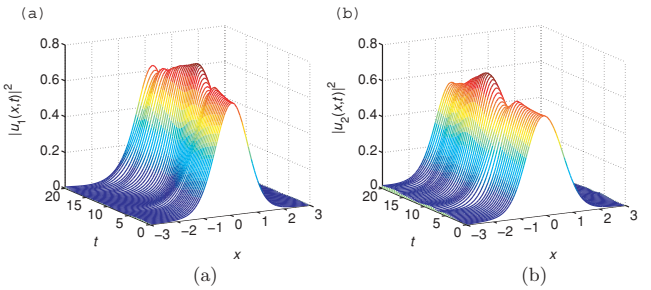

FIG. 8. (Color online) The densities (a) $|u_1(x,t)|^2$ and (b) $|u_2(x,t)|^2$ vs x and t of the two localized BEC states of Fig. 4(b) when the potential parameters are suddenly changed from $\lambda_1 = 8$, $\lambda_2 = 0.862\lambda_1$, $s_1 = 8$, $s_2 = 2.4$ to $\lambda_1 = 8.5$, $\lambda_2 = 0.862\lambda_1$, $s_1 = 8$, $s_2 = 2.4$ at time $t = 5$.

bound due to interspecies attraction even in the absence of the bichromatic OL potential. Hence due to the interspecies attraction, the two localized BEC states tend to overlap and stay together as two bright solitons [26]. In the case represented in Fig. 6(d), g_2 is positive, and the system is less attractive; hence the density distribution is symmetric.

Again it is worthwhile to show the symmetry breaking in a g_2 vs $|g_{12}|$ phase diagram for $g_1 = 0$ as illustrated in Fig. 7. (Similar symmetry breaking has also been studied in the context of symbiotic gap solitons [24].) For small $|g_{12}|$, as expected, the localized states are in a symmetric configuration. The asymmetric configuration is achieved when $|g_{12}|$ is larger than a critical value, indicating that a minimum of attraction is needed to replace the center of the localized states from $x = 0$. Symmetry breaking is favored when the inter- and intraspecies interactions are strongly attractive leading to strong effective attraction in the system; hence it is favored more for large negative (attractive) values of g_2 than for positive (repulsive) values of g_2 as seen in Fig. 7.

C. The stability of the localized BEC states

So far, we have studied the stationary properties of the localized BEC states. Now we investigate if the localized BEC states are stable under small perturbation. We are using real-time propagation routines in the numerical calculation, which usually finds the stable states. This indicates that the localized BEC states we are studying should be stable. However, we now explicitly demonstrate the stability of a set of specific states, e.g., the ones illustrated in Fig. 4(b). To demonstrate that these states are stable, after their formation, we suddenly change the potential parameters from $\lambda_1 = 8$, $\lambda_2 = 0.862\lambda_1$, $s_1 = 8$, $s_2 = 2.4$ to $\lambda_1 = 8.5$, $\lambda_2 = 0.862\lambda_1$, $s_1 = 8$, and $s_2 = 2.4$ and study the resulting dynamics. We plot in Figs. 8(a) and 8(b) the consequent density dynamics $|u_1(x,t)|^2$ and $|u_2(x,t)|^2$ vs x and t, respectively, for $t = 0$–20. The sudden change of the potential is effected at $t = 5$. From Figs. 8(a) and 8(b), we see that at $t = 5$ when the potential is suddenly changed, the density profiles suffer an abrupt change. Nevertheless, the BEC density profiles remain localized for a large interval of time undergoing breathing oscillation, as we can see from Figs. 8(a) and 8(b) for the two components, which demonstrates the stability of the localized BEC states.

IV. SUMMARY

In this paper, using the numerical and variational solution of the time-dependent GP equation, we studied the localization of a two-component cigar-shaped BEC in a quasiperiodic 1D OL potential prepared by two overlapping polarized standing-wave laser beams with different wavelengths and amplitudes. Specifically, we considered two analytical forms (sine and cosine) of the OL potential and considered two distinct cases: (i) the two components under the action of the sine potential (3) and (ii) the sine potential (3) acting on component 1 and the cosine potential (4) acting on component 2. In case (i), for a weak interspecies interaction, both components have a maximum of density at the trap center ($x = 0$) satisfying the symmetry $|u_j(x)|^2 = |u_j(-x)|^2$. In this case the variational analysis is applicable and produced result in good agreement with numerical simulation. In case (ii), for a weak interspecies interaction, one component has a maximum of density at the trap center and the other component has a minimum, however, again satisfying the symmetry $|u_j(x)|^2 = |u_j(-x)|^2$. The localization is most favored for noninteracting atoms and is destroyed in the presence of moderate intraspecies and interspecies repulsive interactions. Here we specially study the effect of weak interspecies and intraspecies nonlinearities on the profile of the localized states. In case (i), for a sufficiently strong interspecies repulsion, the two localized states are found to move in opposite directions from the trap center and attain equilibrium in a separated (split) configuration breaking the symmetry $|u_j(x)|^2 = |u_j(-x)|^2$. In case (ii), for a sufficiently strong interspecies attraction, the two localized states are found to move away from $x = 0$ to the same side of the trap center again breaking the symmetry $|u_j(x)|^2 = |u_j(-x)|^2$. We studied in some detail the formation of the localized states of broken symmetry in all cases considering phase diagram of intra- and interspecies nonlinearities g_2 and g_{12}.

The Anderson localization of a BEC in a bichromatic OL potential as studied here is very distinct from the localization of gap solitons [20,21,36] of the BEC in a monochromatic OL potential. Anderson localization takes place in an aperiodic potential in the linear equation, whereas a periodic potential and a repulsive nonlinearity are crucial for the localization of gap solitons.

We hope that the present work will motivate new studies, specially experimental ones, on the localization of a binary

mixture of BEC in a bichromatic OL potential. The effect of nonlinear interspecies and intraspecies interactions on localization, as investigated in the present paper, also deserves careful analysis.

ACKNOWLEDGMENTS

FAPESP (Brazil) CNPq (Brazil) provided partial support. Y.C. undertook this work with the support of the post-doctoral program of FAPESP (Brazil).

[1] P. W. Anderson, Phys. Rev. **109**, 1492 (1958).
[2] D. S. Wiersma *et al.*, Nature (London) **390**, 671 (1997); F. Scheffold *et al.*, *ibid.* **398**, 206 (1999).
[3] R. Dalichaouch *et al.*, Nature (London) **354**, 53 (1991); A. A. Chabanov *et al.*, *ibid.* **404**, 850 (2000).
[4] R. L. Weaver *et al.*, Wave Motion **12**, 129 (1990).
[5] J. Billy *et al.*, Nature (London) **453**, 891 (2008).
[6] G. Roati *et al.*, Nature (London) **453**, 895 (2008).
[7] J. Chabé, G. Lemarie, B. Gremaud, D. Delande, P. Szriftgiser, and J. C. Garreau, Phys. Rev. Lett. **101**, 255702 (2008).
[8] E. E. Edwards, M. Beeler, T. Hong, and S. L. Rolston, Phys. Rev. Lett. **101**, 260402 (2008).
[9] S. Inouye *et al.*, Nature (London) **392**, 151 (1998).
[10] L. Sanchez-Palencia, D. Clement, P. Lugan, P. Bouyer, G. V. Shlyapnikov, and A. Aspect, Phys. Rev. Lett. **98**, 210401 (2007); D. Clément, A. F. Varon, M. Hugbart, J. A. Retter, P. Bouyer, L. Sanchez-Palencia, D. M. Gangardt, G. V. Shlyapnikov, and A. Aspect, *ibid.* **95**, 170409 (2005); J. E. Lye, L. Fallani, M. Modugno, D. S. Wiersma, C. Fort, and M. Inguscio, *ibid.* **95**, 070401 (2005).
[11] B. Damski, J. Zakrzewski, L. Santos, P. Zoller, and M. Lewenstein, Phys. Rev. Lett. **91**, 080403 (2003); T. Schulte, S. Drenkelforth, J. Kruse, W. Ertmer, J. Arlt, K. Sacha, J. Zakrzewski, and M. Lewenstein, *ibid.* **95**, 170411 (2005).
[12] M. Modugno, New J. Phys. **11**, 033023 (2009); M. Larcher, F. Dalfovo, and M. Modugno, Phys. Rev. A **80**, 053606 (2009).
[13] D. J. Boers, B. Goedeke, D. Hinrichs, and M. Holthaus, Phys. Rev. A **75**, 063404 (2007).
[14] S. K. Adhikari and L. Salasnich, Phys. Rev. A **80**, 023606 (2009).
[15] G. Roux *et al.*, Phys. Rev. A **78**, 023628 (2008).
[16] J. Biddle, B. Wang, D. J. Priour Jr., and S. Das Sarma, Phys. Rev. A **80**, 021603(R) (2009).
[17] A. S. Pikovsky and D. L. Shepelyansky, Phys. Rev. Lett. **100**, 094101 (2008); S. Flach, D. O. Krimer, and Ch. Skokos, *ibid.* **102**, 024101 (2009); I. García-Mata and D. L. Shepelyansky, Phys. Rev. E **79**, 026205 (2009); Ch. Skokos, D. O. Krimer, S. Komineas, and S. Flach, *ibid.* **79**, 056211 (2009); D. L. Shepelyansky, Phys. Rev. Lett. **70**, 1787 (1993); M. Johansson, M. Hornquist, and R. Riklund, Phys. Rev. B **52**, 231 (1995).
[18] T. Roscilde, Phys. Rev. A **77**, 063605 (2008); X. Deng, R. Citro, E. Orignac, and A. Minguzzi, Eur. Phys. J. B **68**, 435 (2009).
[19] T. Paul, M. Albert, P. Schlagheck, P. Leboeuf, and N. Pavloff, Phys. Rev. A **80**, 033615 (2009); T. Paul, P. Schlagheck, P. Leboeuf, and N. Pavloff, Phys. Rev. Lett. **98**, 210602 (2007).
[20] B. Eiermann, Th. Anker, M. Albiez, M. Taglieber, P. Treutlein, K.-P. Marzlin, and M. K. Oberthaler, Phys. Rev. Lett. **92**, 230401 (2004).
[21] B. B. Baizakov, V. V. Konotop, and M. Salerno, J. Phys. B **35**, 5105 (2002); S. K. Adhikari and B. A. Malomed, Europhys. Lett. **79**, 50003 (2007); Physica D **238**, 1402 (2009); E. A. Ostrovskaya and Y. S. Kivshar, Phys. Rev. Lett. **92**, 180405 (2004).
[22] D. S. Hall, M. R. Matthews, J. R. Ensher, C. E. Wieman, and E. A. Cornell, Phys. Rev. Lett. **81**, 1539 (1998).
[23] P. S. Julienne, F. H. Mies, E. Tiesinga, and C. J. Williams, Phys. Rev. Lett. **78**, 1880 (1997).
[24] S. K. Adhikari and B. A. Malomed, Phys. Rev. A **79**, 015602 (2009); **77**, 023607 (2008); A. Gubeskys and B. A. Malomed, *ibid.* **75**, 063602 (2007).
[25] Y. Cheng, J. Phys. B **42**, 205005 (2009).
[26] S. K. Adhikari, Phys. Lett. **A346**, 179 (2005); Phys. Rev. A **72**, 053608 (2005); V. M. Pérez-García and J. B. Beitia, *ibid.* **72**, 033620 (2005).
[27] T. Schwartz *et al.*, Nature (London) **446**, 52 (2007); Y. Lahini, A. Avidan, F. Pozzi, M. Sorel, R. Morandotti, D. N. Christodoulides, and Y. Silberberg, Phys. Rev. Lett. **100**, 013906 (2008).
[28] P. Lugan, D. Clement, P. Bouyer, A. Aspect, and L. Sanchez-Palencia, Phys. Rev. Lett. **99**, 180402 (2007); J. E. Lye, L. Fallani, C. Fort, V. Guarrera, M. Modugno, D. S. Wiersma, and M. Inguscio, Phys. Rev. A **75**, 061603(R) (2007).
[29] C. Fort, L. Fallani, V. Guarrera, J. E. Lye, M. Modugno, D. S. Wiersma, and M. Inguscio, Phys. Rev. Lett. **95**, 170410 (2005); D. R. Grempel, S. Fishman, and R. E. Prange, *ibid.* **49**, 833 (1982); L. Fallani, J. E. Lye, V. Guarrera, C. Fort, and M. Inguscio, *ibid.* **98**, 130404 (2007); P. Lugan, D. Clement, P. Bouyer, A. Aspect, M. Lewenstein, and L. Sanchez-Palencia, *ibid.* **98**, 170403 (2007); N. Bilas and N. Pavloff, Eur. Phys. J. D **40**, 387 (2006).
[30] R. C. Kuhn, C. Miniatura, D. Delande, O. Sigwarth, and C. A. Muller, Phys. Rev. Lett. **95**, 250403 (2005); S. E. Skipetrov, A. Minguzzi, B. A. vanTiggelen, and B. Shapiro, *ibid.* **100**, 165301 (2008); E. Abrahams, P. W. Anderson, D. C. Licciardello, and T. V. Ramakrishnan, *ibid.* **42**, 673 (1979).
[31] C. A. G. Buitrago and S. K. Adhikari, J. Phys. B **42**, 215306 (2009); L. Salasnich, A. Parola, and L. Reatto, Phys. Rev. A **65**, 043614 (2002).
[32] R. Scharf and A. R. Bishop, Phys. Rev. E **47**, 1375 (1993).
[33] V. M. Pérez-García, H. Michinel, J. I. Cirac, M. Lewenstein, and P. Zoller, Phys. Rev. A **56**, 1424 (1997).
[34] Y. Cheng, R. Gong, and H. Li, Opt. Express **14**, 3594 (2006).
[35] P. Muruganandam and S. K. Adhikari, Comput. Phys. Commun. **180**, 1888 (2009).
[36] Z. Shi, K. J. H. Law, P. G. Kevrekidis, and B. A. Malomed, Phys. Lett. **A372**, 4021 (2008).